Chemical Science

rsc.li/chemical-science

Volume 9
Number 1
7 January 2018
Pages 1-268

ISSN 2041-6539

ROYAL SOCIETY
OF CHEMISTRY

EDGE ARTICLE
Xinjing Tang et al.
Caged circular siRNAs for photomodulation of gene
expression in cells and mice

ROYAL SOCIETY
OF CHEMISTRY

rsc.li/chemical-science

ARTICLE

Nature of the Heavy Formal Double Bonds As=Ch, Sb=Ch and Bi=Ch (Ch = S, Se, Te) in NCN-Pincer Supported Arsinidene, Stibinidene and Bismuthinidene Chalcogenides

Fabio Meyer,[a] Arina Siumbeli,[a] Libor Dostál,*[b] Emanuel Hupf*[a] and Jens Beckmann*[a]

The synthesis of an arylpnictinidenes 2,6-(Ph$_2$PNMes)$_2$C$_6$H$_3$Pn based upon a novel bis(phosphine imine) NCN-pincer ligand is reported (Pn = As, Sb, Bi). The oxidation of 2,6-(Ph$_2$PNMes)$_2$C$_6$H$_3$Pn with sulfur, selenium and tellurium, respectively, afforded arylarsinidene chalcogenides 2,6-(Ph$_2$PNMes)$_2$C$_6$H$_3$AsCh, arylstibinidene chalcogenides 2,6-(Ph$_2$PNMes)$_2$C$_6$H$_3$SbCh and arylbismuthinidene chalcogenides 2,6-(Ph$_2$PNMes)$_2$C$_6$H$_3$SbCh, which can be formulated as containing terminal Sb=Ch and Bi=Ch double bonds. Based on the complementary bonding analysis, the bonding situation is best described in terms of bipolar $^+$Pn–Ch$^-$ single bonds (Ch = S, Se, Te).

Introduction

Arylpnictinidenes, RPn (Pn = N, P, As, Sb, Bi; R = aryl), are neutral carbene analogues of group 15[1,2] that received tremendous attention in recent years owing to their low valency and arising opportunities for main group driven bond activation and catalysis.[3,4] In their native form, arylpnictinidenes, are fiercely reactive species due to their electron deficiency as well as their electronic triplet ground states and only very recently, it has been discovered that *kinetic stabilization* of triplet arylpnictinidenes, can be achieved using extremely bulky and rigid M^{S}Fluind substituents that effectively shield the pnictogen atoms.[5-9] Predating this discovery, singlet arylpnictinidenes were obtained by *electronic stabilization* using intramolecularly coordinating aryl substituents comprising N-donor atoms, which are able to compensate the electron deficiency of the pnictogen atoms. In 2010, the first isolable arylstibinidene and arylbismuthinidene, 2,6-[RNC(R')]$_2$C$_6$H$_3$E (I: Pn = Sb, Bi; R = 2,6-Me$_3$C$_6$H$_3$, R' = Me) were reported using an adjustable bis(aldimine) and bis(ketimine)-based NCN-pincer ligand system (Scheme 1).[10] Structural elucidation revealed that both N atoms are involved into the coordination of the pnictogens giving rise to formal hypervalent bonding. Since then, closely related arylstibinidenes and -bismuthinidenes I were reported with the same NCN-pincer ligand system, at which the positions of the organic substituents R and R' were varied with the aim of fine tuning the reactivity.[11-14]
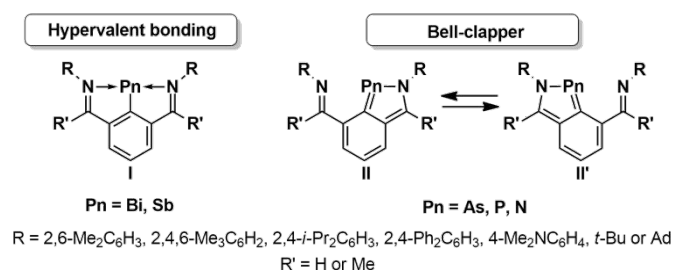
Scheme 1 Electronically stabilized arylpnictinidenes containing NCN-pincer ligands.

The lighter group 15 analogues, namely arylnitrenes, -phosphinidenes and -arsinidenes II were reported with the same bis(imine)-based NCN-pincer ligand system.[14-19] Notably, within the lighter arylpnictindenes, one imine-group preferentially coordinates to the pnictogens due to the smaller size and aromatic stabilization of the resulting five-membered heterocycles, while a fluxional exchange ("bell-cappers") was observed in solution. Asymmetric coordination modes may be locked in upon modification of the NCN-pincer system.[11,14,20,21] The arylpnictinidenes I and II were subject to extensive reactivity studies. The heavier arylpnictinidenes 2,6-[RNC(H)]$_2$C$_6$H$_3$Pn (Pn = As, Sb, Bi) were used as donor ligands for the preparation of numerous metal carbonyl complexes of Cr, Mo, W, Fe, Mn and Co[12,16] as well as Au.[22] or in Diels-Alder type cycloadditions with alkynes.[26, 27] The stibinidene 2,6-[t-BuNC(H)]$_2$C$_6$H$_3$Sb was utilized as effective main group redox catalyst in the hydroboration of disulfides[29] as well as in reversible addition reactions with N-alkyl/arylmaleimides.[28] The bismuthinidenes 2,6-[RNC(H)]$_2$C$_6$H$_3$Bi undergoes (light assisted) oxidative addition with aryl iodides,[23,24] stemming from single-electron transfer (SET) processes.[25] Activation of dinitrogen oxide provided an asymmetric oxidation product,[13] which was able to oxidize HBpin to HOBpin. Reaction of the bismuthinidene 2,6-[2',6'-Ph$_2$C$_6$H$_3$NC(Me)]$_2$C$_6$H$_3$Bi with the

[a.] Institute for Inorganic Chemistry and Crystallography, University of Bremen,
[b.] Leobener Straße 7, 28359 Bremen, Germany.
[c.] Department of General and Inorganic Chemistry, Faculty of Chemical Technology, University of Pardubice, Studentska, 573, Pardubice 532 10, Czech Republic.

ARTICLE

2,4,6-tri-*tert*-butylphenoxy radical gave rise to a Bi(III) species featuring an extremely labile Bi–O bond, which could be readily transformed into an arylbismuth(II) species able to activate protic species, such as water, ammonia, phenol and aniline.[30] Furthermore, upon single electron oxidation with [Cp$_2$Fe][BArF$_4$], the arylbismuthinidene could be converted into the related radical cations.[31] The utility of the arylbismuthinidene 2,6-[*t*-BuNC(H)]$_2$C$_6$H$_3$Bi as catalyst was showcased for transfer hydrogenation reactions of azobenzenes,[32] which occurs without metal-ligand cooperativity,[20] the hydrodefluorination of polyfluorinated aromatics[33] as well as for the degradation of sulfur hexafluoride and phenylsulfur pentafluoride.[34] Most recent applications in catalysis include light-induced trifluoro-methylation of heteroarenes,[35] light-induced reductive cyclo-propanation of alkenes with diiodomethane and manganese powder[36] as well as the intramolecular aminocyclization affording cyclic carbamates.[37]

Given the rich diversity in the reactivity of stibinidenes and bismuthinidenes as well as the non-innocent character of the bis(aldimine) and bis(ketimine)-based NCN-pincer ligand system, we envisaged a novel bis(phosphine imine)-based NCN-pincer scaffold, derived from the 2,6-[bis(diphenylphosphino-phenyl)]phenyl substituent, recently introduced by us and applied for the synthesis of transition metal complexes.[38-40] This novel bis(phosphine imine)-based NCN-pincer scaffold based upon PNMes groups allowed the preparation of a novel arsinidene, stibinidene and bismuthinidene, the oxidation of which with chalcogens gave rise to the formation of *electronically stabilized* stibinidene chalcogenides and bismuthinidene chalcogenides comprising formal As=Ch, Sb=Ch and Bi=Ch double bonds (Ch = S, Se, Te) including the first structurally authenticated Bi=Te double bond. These compounds nicely complement the *kinetically stabilized* stibinidene chalcogenides reported very recently.[41]

Results & Discussion

Synthetic Aspects

The ligand precursor was synthesized by a Staudinger reaction of 2,6-(Ph$_2$P)$_2$C$_6$H$_3$Br[42] with two equivalents of mesityl azide to provide 2,6-(Ph$_2$PNMes)$_2$C$_6$H$_3$Br (**1**) as colourless crystals in 84% yield (Scheme 2). The ^{31}P NMR spectrum of **1** consists of a singlet at δ = −8.9 ppm, which is more deshielded compared to related pincer complexes reflecting the relative coordination strengths of the N atoms, *vide infra*.

The metal halide exchange reaction of **1** with the Turbo-Grignard-reagent, *i*-PrMgCl·LiCl, produced the arylmagnesium chloride 2,6-(Ph$_2$PNMes)$_2$C$_6$H$_3$MgCl·THF·Et$_2$O (**2**) as pale-yellow crystals in 90% yield (Scheme 3). The molecular structures of **1** and **2** are shown in Figure 1. As anticipated, the N atoms of **1** are not involved in any interactions with the Br atom. The short, unaltered P–N bond lengths of **1** (1.546(2), 1.548(2) Å) may be regarded as reference values for the discussion of the relative coordination strengths in related pincer complexes, *vide infra*.
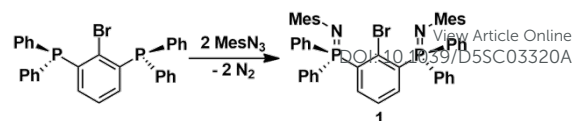
Scheme 2   Synthesis of **1**.
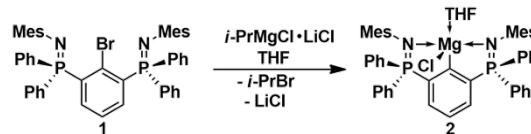
Scheme 3   Synthesis of **2**.

In **2**, both N atoms firmly coordinate to the Mg atom, leading to a tetrahedral spatial arrangement of the Mg atom in **2**, defined by a CN$_2$O donor set. The Mg–N bond lengths (2.222(2), 2.248(2) Å) are marginally unequal. As the result of this coordination, the P–N bond lengths of **2** (1.596(2), 1.598(2) Å) are slightly longer than in **1**. Additionally, **2** shows a ^{31}P-NMR chemical shift of 10.0 ppm.

The salt metathesis reaction of **2** with pnictogen trichlorides, PnCl$_3$ (Pn = P, As, Sb, Bi) afforded the aryldichloropnictogens, 2,6-(Ph$_2$PNMes)$_2$C$_6$H$_3$PnCl$_2$ (**3Pn**) as colourless crystalline solids in 61-94% yield (Scheme 4). Unlike **3As**, **3Sb** and **3Bi** that are indefinitely stable when kept under inert conditions, **3P** decomposes within a few days into ill-defined products even when stored as solid under argon.

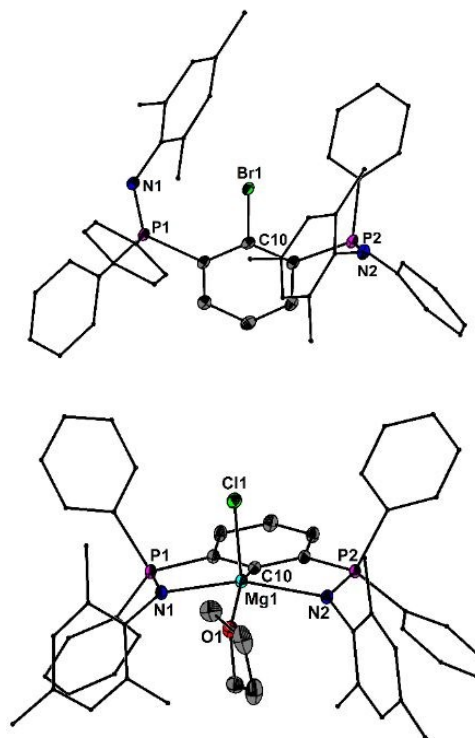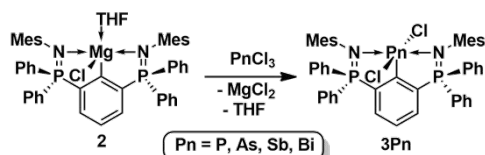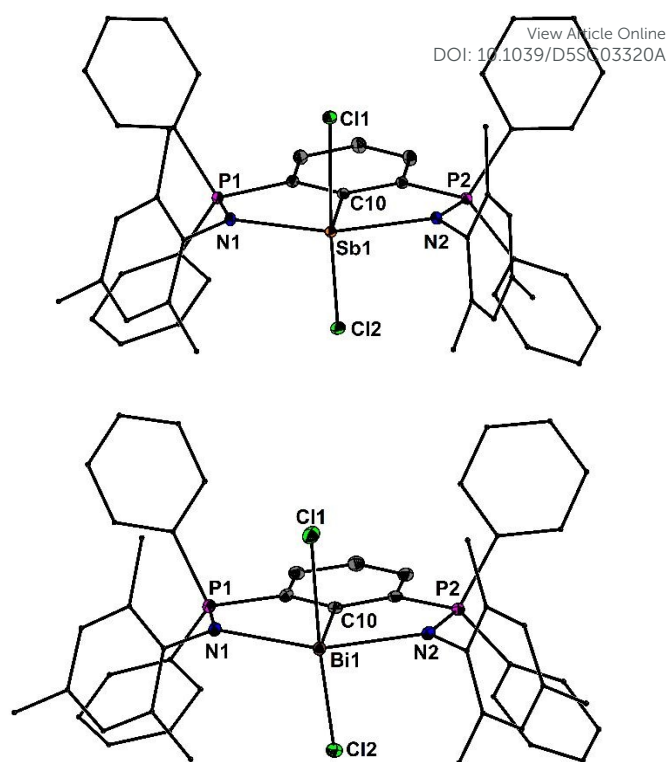**Figure 1.** Molecular structures of **1** and **2** showing 50% probability ellipsoids and the essential atomic numbering scheme of the core region. Substituents are shown as wireframe for clarity. Selected bond lengths [Å] for **1**: P1-N1 1.546(2), P2-N2 1.548(2); for **2**: P1-N1 1.596(2), P2-N2 1.598(2), Mg1-N1 2.222(2), Mg1-N2 2.248(2), Mg1-C10 2.130(2), Mg1-Cl1 2.381(1), Mg1-O1 2.073(2)

Journal Name

Scheme 4. Synthesis of **3Pn** (E = P, As, Sb, Bi)

Scheme 5. Synthesis of [**4Pn**][A] (Pn =P, As, Sb, Bi; A = O$_3$SCF$_3$, AlCl$_4$).

The molecular structures of **3Sb** and **3Bi** are shown in Figure 2. The spatial arrangement of the Sb and Bi atoms is distorted square pyramidal due to the stereochemically active lone pairs and defined by CN$_2$Cl$_2$ donors sets. The Sb–N and Bi–N bond lengths of **3Sb** (2.286(1), 2.326(1) Å) and **3Bi** (2.395(2), 2.438(2) Å) are slightly unequal and significantly shorter than those of the arylantimony- and -bismuth dichlorides 2,6-(t-BuNCH)$_2$C$_6$H$_3$PnCl$_2$ (Sb: 2.415(2), 2.399(2) Å, Bi: 2.470(7), 2.499(6) Å).[43] In turn, the Sb–Cl and Bi–Cl bond lengths of **3Sb** (2.605(1), 2.693(1) Å) and **3Bi** (2.626(1), 2.849(1) Å) are slightly longer than those of 2,6-(t-BuNCH)$_2$C$_6$H$_3$PnCl$_2$ (Sb: 2.597(1), 2.583(1) Å; Bi: 2.662(2), 2.689(2) Å).[43] Based upon the comparison of the P–N bond lengths, the N-coordination in **3Sb** (1.604(2), 1.600(1) Å) is somewhat stronger than in **3Bi** (1.595(2), 1.596(2) Å), which reflects the greater Lewis acidity of the Sb compound. The phosphine imide moieties give rise to ^{31}P NMR chemical shifts of δ = 19.8 (**3P**), 21.1 (**3As**), 22.9 (**3Sb**) and 37.6 ppm (**3Bi**), respectively. The central P-atom of **3P** revealed a triplet centred at δ = 100.0 ppm with a J(^{31}P-^{31}P) coupling of 46 Hz. Despite arduous efforts, we failed to obtain single crystals of **3P** and **3As**. On one occasion, we obtained a small crop of crystals that was identified as the arylchloroarsenium ion, [2,6-(Ph$_2$PNMes)$_2$C$_6$H$_3$AsCl][As$_2$OCl$_5$] [**4As**][As$_2$OCl$_5$], which serendipitously formed from **3As**, excess AsCl$_3$ and adventitious moisture.

In an effort to deliberately prepare arylchloropnictogenium ions, we reacted the aryldichloropnictogens **3Pn** (Pn = P, As, Sb, Bi) with trimethylsilyl triflate, Me$_3$SiO$_3$SCF$_3$, or aluminium trichloride, AlCl$_3$ (Scheme 5). Both Lewis acids abstracted a chloride giving rise to the formation of the desired arylchloropnictogenium ions [2,6-(Ph$_2$PNMes)$_2$C$_6$H$_3$PnCl][A] ([**4Pn**]A, Pn = P, As, Sb, Bi; A$^-$ = O$_3$SCF$_3$$^-$, AlCl$_4$$^-$) that were isolated as colourless crystalline solids in quantitative yields. The molecular structures of [**4As**]$^+$ and [**4Sb**]$^+$ are depicted in Figure 3. The spatial arrangement of the As and Sb atoms is distorted disphenoidal due to the stereochemically active lone pairs and defined by CN$_2$Cl donor sets.
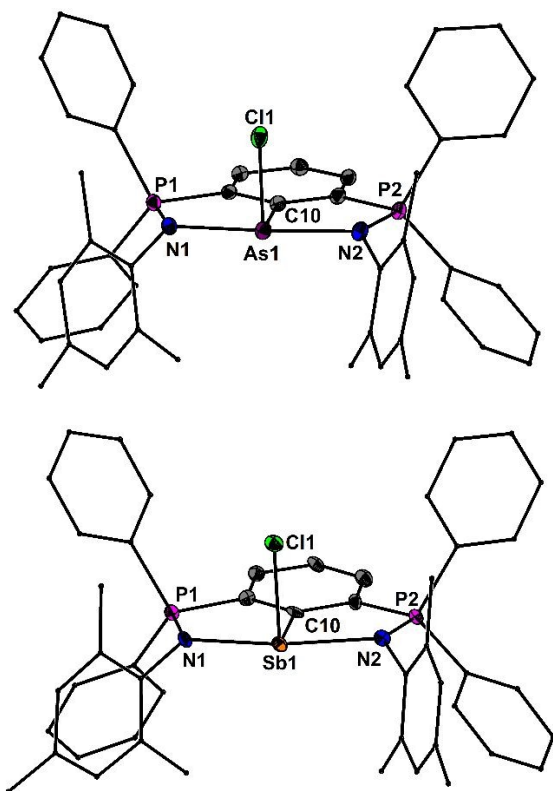

Figure 2. Molecular structures of **3Sb** and **3Bi** showing 50% probability ellipsoids and the essential atomic numbering scheme of the core region. Substituents are shown as wireframe for clarity. Selected bond lengths [Å] for **3Sb**: P1-N1 1.604(2), P2-N2 1.600(1), Sb1-N1 2.286(1), Sb1-N2 2.326(1), Sb1-C10 2.129(2), Sb1-Cl1 2.605(1), Sb1-Cl2 2.693(1); for **3Bi**: P1-N1 1.595(2), P2-N2 1.596(2), Bi1-N1 2.438(2), Bi1-N2 2.395(2), Bi1-C10 2.219(3), Bi1-Cl1 2.626(1), Bi1-Cl2 2.849(1).

The Sb–N bond lengths of [**4Sb**]$^+$ (2.226(5), 2.272(6) Å) are slightly shorter than those of **3Sb** (2.286(1), 2.326(1) Å) and the remaining Sb–Cl bond length [**4Sb**]$^+$ (2.410(2) Å) is shorter than those in **3Sb** (2.605(1), 2.693(1) Å), but longer than in the chlorostibenium cations [2,6-(t-BuNCH)$_2$C$_6$H$_3$SbCl]$^+$ (2.360(1) Å) and [2,6-(2',6'-Me$_2$C$_6$H$_4$NCH)$_2$C$_6$H$_3$SbCl]$^+$ (2.361(1) Å).[44] Based upon the P–N bond lengths of [**4As**]$^+$ (1.597(6), 1.601(6) Å) and [**4Sb**]$^+$ (1.600(1), 1.601(6) Å), the N-coordination within these two cations is very similar, but slightly stronger than in **3Sb** and **3Bi**, vide supra. Interestingly, the two mesityl groups and the two P atoms of the complete series [**4Pn**]$^+$ (Pn = P, As, Sb, Bi) are magnetically inequivalent in solution. The ^{31}P NMR spectrum of [**4P**]$^+$ gives rise to three equally intense signals at δ = 129.4 59.3 and 33.0 ppm. The first two signals comprise doublets with J(^{31}P-^{31}P) couplings of 62 and 62 Hz, while the last signal is a singlet, which suggest an unsymmetrical coordination mode in solution. Consistently, the remaining compounds show pairs of ^{31}P NMR signals at δ = 60.0 / 33.7 ([**4As**]$^+$), 60.0 / 30.0 ([**4Sb**]$^+$) and 78.2 / 37.5 ppm for ([**4Bi**]$^+$), respectively.

The reduction of the heavier aryldichloropnictogens **3Pn** (Pn = As, Sb, Bi), with Li[Et$_3$BH] provided the arylpnictinidenes 2,6-(Ph$_2$PNMes)$_2$C$_6$H$_3$Pn (**5Pn**) as red solids in quantitative yields (Scheme 6). Alternatively, the arylstibinidene 2,6-(Ph$_2$PNMes)$_2$C$_6$H$_3$Sb (**5Sb**) was also obtained by the reduction of **3Sb** with LiAlH$_4$ and isolated as **5Sb**·(AlCl$_3$·THF)·THF.

Figure 3. Molecular structures of [**4As**]⁺ and [**4Sb**]⁺ showing 50% probability ellipsoids and the essential atomic numbering scheme of the core region. Substituents are shown as wireframe for clarity. Selected bond lengths [Å] for [**4As**]⁺: P1-N1 1.605(3), P2-N2 1.601(3), As1-N1 2.122(3), As1-N2 2.114(3), As1-C10 1.967(3), As1-Cl1 2.242(1); for [**4Sb**]⁺: P1-N1 1.601(6), P2-N2 1.597(6), Sb1-N1 2.226(5), Sb1-N2 2.272(6), Sb1-C10 2.158(6), Sb1-Cl1 2.410(2).
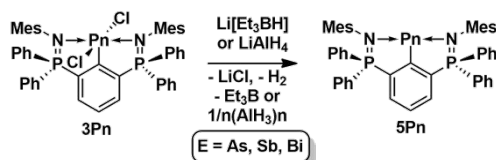

Scheme 6. Synthesis of **5Pn** (Pn = As, Sb, Bi).

Notably, neither the donor acceptor complex $AlCl_3 \cdot THF$ nor the free THF showed any coordination to the Sb atom, but facilitated crystallization. Unfortunately, the arylpnictinidenes are thermally unstable and start to decompose within few hours under argon. While attempting to grow single crystals of the arylbimuthinidene 2,6-$(Ph_2PNMes)_2C_6H_3Bi$ (**5Bi**), a small crop a crystalline decomposition product was obtained, namely the arlyalkylbismuthenium ion [2,6-$(Ph_2PNMes)_2C_6H_3BiEt][Et_4B]$ (Figure S128), which formed via oxidative addition of the ethylboron species and ethyl group scrambling. Interestingly, all attempts to prepare **5Sb** using $NaBH_4$ as reducing agent gave the donor acceptor complex **5Sb**·BH_3 as unstable red crystals. The reaction of **5Sb** with $BH_3 \cdot THF$ provided the same complex **5Sb**·BH_3 that was isolated quantitatively, while **5Bi** showed no reactivity towards $BH_3 \cdot THF$ (Scheme 7).
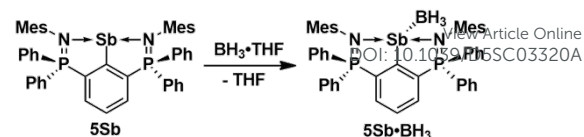
Scheme 7. Synthesis of **5Sb**·BH_3.
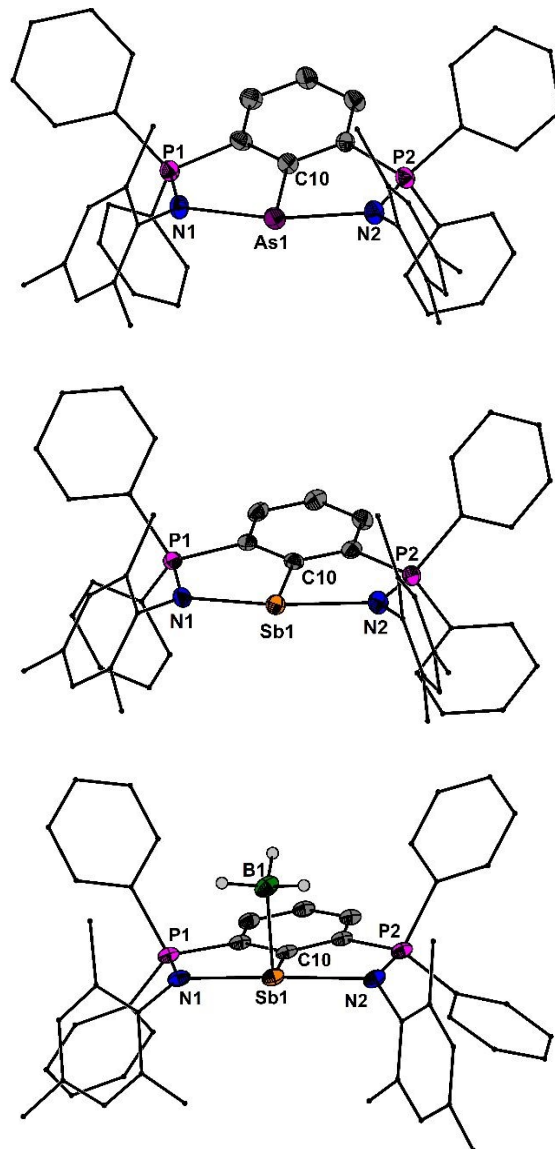
Figure 4. Molecular structures of **5As**, **5Sb** and **5Sb**·BH_3 showing 50% probability ellipsoids and the essential atomic numbering scheme. Selected bond lengths [Å] for **5As**: P1-N1 1.592(3), P2-N2 1.586(3), As1-N1 2.242(3), As1-N2 2.271(3), As1-C10 1.900(4). Selected bond lengths [Å] for **5Sb**: P1-N1 1.610(3), P2-N2 1.600(3), Sb1-N1 2.273(3), Sb1-N2 2.312(3), Sb1-C10 2.155(3). Selected bond lengths [Å] for **5Sb**·BH_3: P1-N1 1.590(3), P2-N2 1.585(3), Sb1-N1 2.337(3), Sb1-N2 2.361(3), Sb1-C10 2.163(3), Sb1-B1 2.293(4).

So far, all attempts to reduce **3P** with various reducing agents, such as KC_8, lithium, potassium, $Li[Et_3BH]$ or Cp_2Co, gave only ill-defined mixture of products. The molecular structures of **5As**, **5Sb** and **5Sb**·BH_3 are shown in Figure 4. The As-N bond lengths of **5As** (2.242(3), 2.271(3) Å) are longer than those of the arylchloroarsenium ion [**4As**]⁺ (2.122(3), 2.114(3) Å). The Sb–N

bond lengths of the arylstibinidene **5Sb** (2.273, 2.272(6) Å) are between those of the arylantimony dichloride **3Sb** (2.286(1), 2.326(1) Å) and the arylchlorostibenium ion [**4Sb**]⁺ (2.226(5), 2.272(6) Å). The Sb–N bond lengths of the donor acceptor complex **5Sb**·BH₃ (2.337(3), 2.361(3) Å) are substantially longer, which suggests a lower Lewis acidity than in the aforementioned antimony compounds. This is also reflected in the short P–N bond lengths of **5Sb**·BH₃ (1.585(3), 1.590(3) Å). Notably, the Sb–N bond lengths of the 2,6-bis[N-2',6'-(dimethylphenyl)ketimino]stibinidene (2.352(3), 2.346(3) Å) are in between those of **5Sb** and **5Sb**·BH₃. The donor acceptor Sb–B bond of **5Sb**·BH₃ (2.293(4) Å) compares well with the sum of covalence radii. The ³¹P NMR resonances of **5Sb**, **5Sb**·BH₃ and **5Bi** show little variance at δ = 10.8, 16.0 and 8.8 ppm.

The reaction of the arylarsinidene **5As**, arylstibinidene **5Sb** and the arylbismuthinidene (**5Bi**) with sulfur, selenium and tellurium gave rise to the formation of arylarsinidene **5As**, chalcogenides, 2,6-(Ph₂PNMes)₂C₆H₃AsCh (**6AsCh**; Ch = S, Se), arylstibinidene chalcogenides, 2,6-(Ph₂PNMes)₂C₆H₃SbCh (**6SbCh**; Ch = S, Se, Te), and arylbismuthinidene chalcogenides, (Ph₂PNMes)₂C₆H₃BiCh (**6BiCh**; Ch = S, Se, Te), which were isolated as yellow (**6AsS**, **6AsSe**, **6SbS**, **6SbSe** and **6BiS**, **6BiSe**) and red (**6SbTe** and **6BiTe**) crystalline needles in nearly quantitative yield based on ³¹P-NMR (Scheme 8). The molecular structures of **6AsSe**, **6SbSe** and **6BiTe** are shown in Figure 5. The As–Se bond length of **6AsSe** (2.310(1) Å) is marginally smaller than that of 2,6-(Me₂NCH₂)₂C₆H₃AsSe (2.351(3) Å).[45] The Sb–Se bond length of **6SbSe** (2.466(1) Å) is marginally larger those in the *electronically stabilized* species 2-[(2',4'-*i*-Pr₂C₆H₄)NC(H)]-6-[(2'',4''-*i*-Pr₂C₆H₄)NHC(H)]C₆H₃SbSe (2.437(1) Å)[14], [2,6-(Me₂NCH₂)C₆H₃]SbSe (2.440(1) Å) and 2,6-[2',6'-Ph₂C₆H₃NC(Me)]₂C₆H₃SbSe (2.433(1) Å)[46] and substantially longer than in the *kinetically stabilized* MˢFluind*SbSe (2.372(1) Å).[41] The Bi-Te bond length of **6BiTe** (2.7614(4) Å) is the longest formal double bond ever reported. It is considerably shorter than the single bond lengths of Et₂BiTeEt (2.912(1) Å)[47] and 2-[(2',4'-*i*-Pr₂C₆H₄)NC(H)]C₆H₃Bi(TePh)₂ (2.895(1) Å).[48] The ³¹P NMR chemical shifts of **6AsCh**, **6SbCh** and **6BiCh** are in the range from δ = 12.9 to 13.2 ppm, from δ = 14.6 to 15.6 ppm and from δ = 18.2 to 22.8 ppm, respectively. Despite all efforts, no ⁷⁷Se NMR signals were found for the selenides **6AsSe**, **6SbSe** and **6BiSe** after scanning the range from −3000 to +6000 ppm for several hours. The ¹²⁵Te NMR spectra of the tellurides **6SbTe** and **6BiTe** gave rise to singlets at δ = −274.8 and −193.1 ppm.

DFT Computations

In an effort to unravel the nature of the heavy As=Ch, Sb=Ch and Bi=Ch double bonds in the arylpnictinidene chalcogenides, 2,6-(Ph₂PNMes)₂C₆H₃AsCh (**6AsCh**; Ch = S, Se, Te), 2,6-(Ph₂PNMes)₂C₆H₃SbCh (**6SbCh**; Ch = S, Se, Te), (Ph₂PNMes)₂C₆H₃BiCh (**6BiCh**; Ch = S, Se, Te) we performed a complementary bonding analyses.[49]
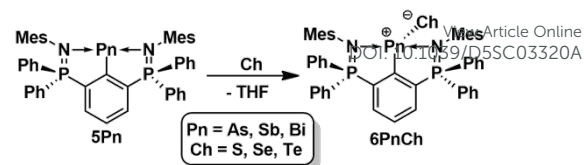
Scheme 8. Synthesis of **6PnCh** (Pn = As, Sb, Bi; Ch = S, Se, Te).
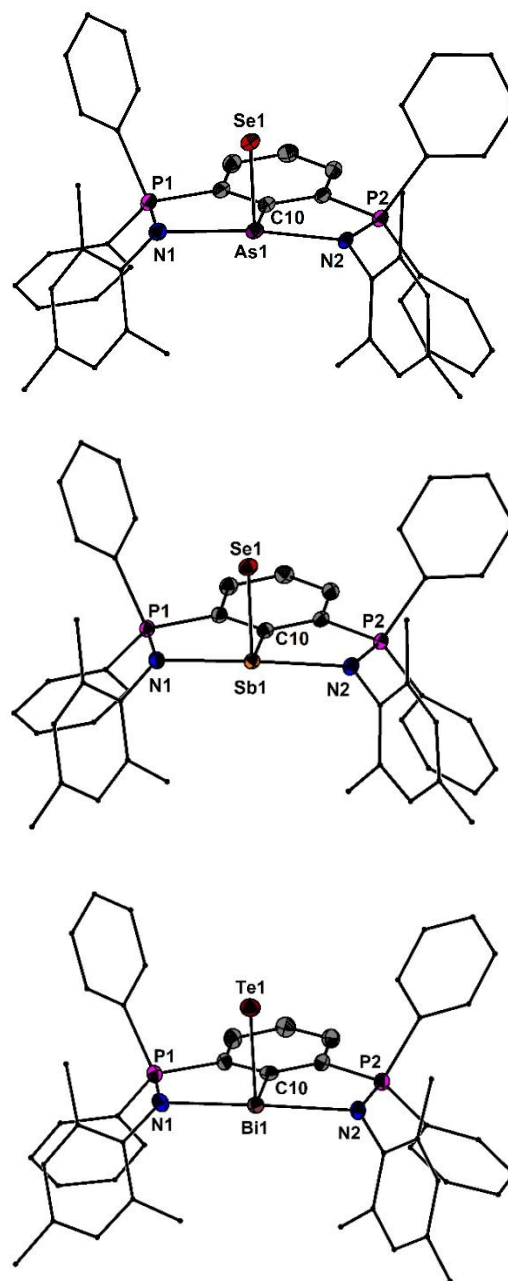
Figure 5. Molecular structures of **6AsSe**, **6SbSe** and **6BiTe** showing 50% probability ellipsoids and the essential atomic numbering scheme of the core region. Substituents are shown as wireframe for clarity. Selected bond lengths [Å] for **6AsSe**: P1-N1 1.569(2), P2-N2 1.605(2), As1-N1 2.376(2), As1-N2 2.126(2), As1-C10 2.000(2), Se1-As1 2.310(1). Selected bond lengths [Å] for **6SbSe**: P1-N1 1.584(1), P2-N2 1.597(1), Sb1-N1 2.386(1), Sb1-N2 2.307(1), Sb1-C10 2.189(1), Sb1-Se1 2.4661(2). Selected bond lengths [Å] for **6BiTe**: P1-N1 1.582(4), P2-N2 1.586(4), Bi1-N1 2.499(4), Bi1-N2 2.488(3), Bi1-C10 2.306(4), Bi1-Te1 2.7614(4).

ARTICLE

The electron density-based Atoms-In-Molecule (AIM)[50] approach reveal decreasing electron density values (ρ_{bcp}) at the bond critical point with increasing size of the chalcogen of 0.86/0.70/0.65 e Å^{-3} (AsS/SbS/BiS), 0.72/0.61/0.57 e Å^{-3} (AsSe/SbSe/BiSe) and 0.56/0.50/0.47 e Å^{-3} (AsTe/SbTe/BiTe) with slightly higher values obtained for **6AsCh**. Interestingly, the Laplacians ($\nabla^2\rho_{bcp}$) are increasing from AsS to AsTe, while a steady decrease is observed for the heavier congeners SbS to SbTe as well as from BiS to BiTe indicating an increase in ionic contributions for **6AsCh** and a decrease within **6SbCh** and **6BiCh**. However, the kinetic energy over electron density ratios (G/ρ_{bcp}) are slightly steadily decreasing also from AsS to AsTe indicating a slight decrease in ionic bonding contributions also for **6AsCh** (Table S2 to S4). On the other side, the total energy over electron density values (H/ρ_{bcp}) are getting closer to zero from S to Te, which in turn indicate a simultaneous slight increase in polarity/iconicity also for the heavier **6SbCh** and **6BiCh**. Such behavior has also been described before for Si–O bonds.[51] Despite the rather low values of AIM derived parameters, the delocalization indices ranging from 1.19 to 1.26 for AsCh, 1.24 to 1.26 for SbCh and from 1.29 to 1.30 for BiCh supporting the formulation of formal Ch=Pn double bonds (Table S5). The Wiberg Bond indices (WBI, AsCh: 1.11-1.23, SbCh: 1.19-1.21; BiCh: 1.21-1.25) are lower compared to the recently reported *kinetically stabilized* stibinidene chalcogenides M^{S}Flunid*SbCh (ranging from 1.69 to 1.82)[41] presumably owing to the electronic stabilization of the N-atoms in **6PnCh**. Inspection of the Non-covalent interaction (NCI) index clearly indicates the covalent bonding contributions along the SbCh and BiCh bond axis, which are visibly more pronounced within the AsS interactions already indicated by the AIM paramters (Figure 6, S129 to S131).[52] Furthermore, the trend in AIM parameters for the series **6PnCh** augment the values reported for the heaviest members of SbO and BiO bonds being prepared only recently.[53,54] Following the trend, the SbO and BiO bcp show the highest values of ρ_{bcp} and $\nabla^2\rho_{bcp}$ indicating a higher degree of polarity in the oxygen based SbO and BiO double bonds. Extending the analysis of ρ_{bcp}, $\nabla^2\rho_{bcp}$ and the ellipticity (ϵ) along the entire PnCh bond lengths reveal a substantial difference between the PnS bonds and the heavier PnSe and PnTe bonds. The electron density along the AsS, SbS and BiS bonds are asymmetric (Figure S132), reminiscent of the reported AsO, SbO and SbO bonds,[53] whereas the distribution of ρ becomes more symmetric for the heavier chalcogens Se and Te (Figure S132). The Laplacians of ρ show a clear minimum near the sulfur in all PnS bonds, again similar to the respective heavier PnO bonds,[53] which is absent in the PnSe and PnTe bonds. However, slight differences are observed between the AsSe and AsTe bonds compared to the heavier analogues. For AsSe, $\nabla^2\rho_{bcp}$ is almost symmetrically distributed, whereas a small minimum is formed in the location of the selenium for SbSe and BiSe. For AsTe, $\nabla^2\rho_{bcp}$ a small minimum is observed in the location of the arsenic, whereas for SbTe the distribution is rather symmetric and for BiTe a small minimum is observed on the direction of the tellurium (Figure S132).
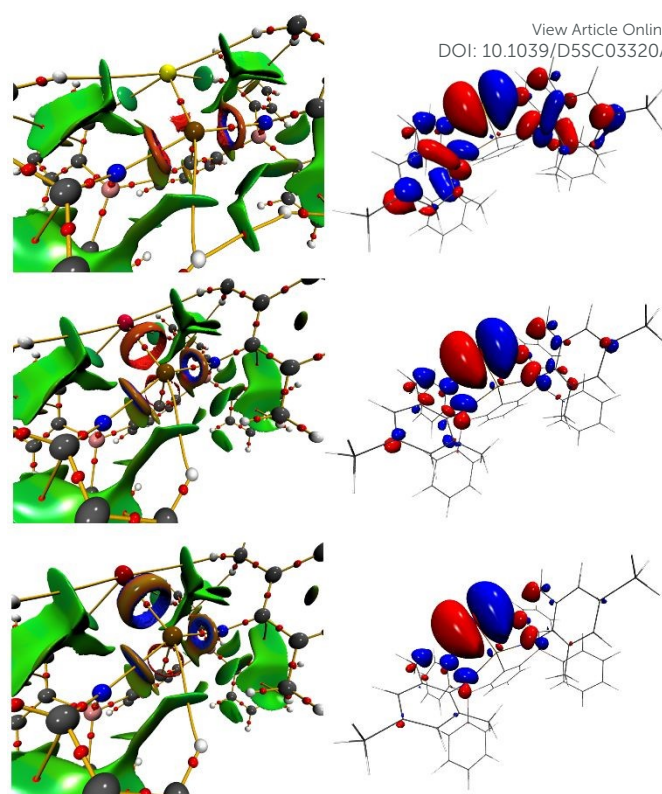
Figure 6. AIM molecular graphs of **6SbSe** (top left) and **6BiTe** (bottom left) with bond critical points as red spheres and bond paths in orange as well as NCI *iso*-surfaces at s(r) = 0.5 colour coded with sign(λ2)ρ in a. u. Blue surfaces refer to attractive forces and red to repulsive forces. Green indicates weak interactions. Respective HOMO–1 of **6SbSe** (top right) and **6BiTe** (bottom right) at *iso*-surfaces at s(r) = +/– 0.02 (blue/red).

For the ellipticity, the highest values are observed close to the arsenic in the AsCh bonds, which decrease towards the bond critical point and reach a minimum after the bcp before increasing towards the chalcogens. For the SbCh and BiCh bonds, the overall ellipticities are substantially smaller, with the SbCh bonds showing the same trend as the AsCh bonds. For the BiCh bonds, the ellipticities reach a minimum before the bcp (closer to the bismuth) and increase towards the chalcogen (Figure S132). NBO/NLMO analyses of the SbCh and BiCh bonds revealed in each case only one Sb–Ch and Bi–Ch bonding orbital in line with the formulation of bipolar $^+$Sb–Ch$^-$ and $^+$Bi–Ch$^-$ bonds (Table S7, S9 and S11).[55] Second-order perturbation theory shows LP(Ch) → LV(Sb/Bi), LP(Ch) → LV(C$_{ipso}$) and LP(Ch) → σ*(Sb/Bi–C) donor-acceptor interactions summing up to a total of E2 = 63 to 73 kcal mol^{-1} (**6AsCh**), E2 = 48 to 53 kcal mol^{-1} (**6SbCh**) and E2 = 41 to 46 kcal mol^{-1} (**6BiCh**), which are higher compared to values reported for the SbO and BiO bonds.[54] The NLMO analysis revealed that two LP_Ch NLMOs show reduced percentages of the parent NBO, indicating that the respective lone pairs are partially delocalized and make up 12.4 to 17.4 % (**6AsCh**), 15.4 to 20.1 % (**6SbCh**) and 20.8 to 25.5 % (**6BiCh**) of the total AsCh/SbCh/BiCh NLMO bond orders (Tables S5, S8, S10 and S12). The partial π-backdonation from the chalcogen is also visible in the respective HOMO–1 molecular orbitals (Figures 6, S136 to S138). Additionally, EDA-NOCV[56] analyses of the two experimentally obtained molecular structures of **6SbSe** and

Journal Name

ARTICLE

6BiTe were carried out considering two different bonding situations: (i) For the interaction of the formal Sb=Se and Bi=Te double bond, two neutral fragments in their respective triplet states have been applied. (ii) For the bipolar bonding situation $^+$Sb–Se$^-$ and $^+$Bi–Te$^-$, charged fragments (RSb$^+$/RBi$^+$ and Se$^-$/Te$^-$) in their respective doublet state have been used. The energy terms derived from the EDA-NOCV analysis are summarized in Table S10. The bipolar bonding situation with a Sb–Se and Bi–Te single bond give rise to ΔE_{orb} values which are closer to zero compared to the ΔE_{orb} values obtained for the double bond situation, indicating that the heavy formal double bonds are better described with a Lewis structure containing bipolar $^+$Pn–Ch$^-$ bonds. As a last point, the *iso*-surface of the localized orbital locator[57] of the π-orbitals (LOL-π), exemplified for **6BiCh** show the same trend (Figure S140) clearly indicating a charge separated formulation with pi-electron residing at the chalcogens, respectively.

Conclusions

A novel NCN-pincer ligand based upon a bis(phosphine imine) substituted phenyl substituent was introduced and applied for the preparation of an *electronically stabilized* arylarsinidene 2,6-(Ph$_2$PNMes)$_2$C$_6$H$_3$As (**5As**), arylstibinidene 2,6-(Ph$_2$PNMes)$_2$C$_6$H$_3$Sb (**5Sb**) and arylbismuthinidene 2,6-(Ph$_2$PNMes)$_2$C$_6$H$_3$Bi (**5Bi**). The oxidation of **5As**, **5Sb** and **5Bi** with sulfur, selenium and tellurium, respectively, produced the arylarsinidene chalcogenides 2,6-(Ph$_2$PNMes)$_2$C$_6$H$_3$AsCh (**6AsCh,** Ch = S, Se), arylstibinidene chalcogenides 2,6-(Ph$_2$PNMes)$_2$C$_6$H$_3$SbCh (**6SbCh**) and arylbismuthinidene chalcogenides 2,6-(Ph$_2$PNMes)$_2$C$_6$H$_3$BiCh (**6BiCh**) formally containing terminal Sb=Ch and Bi=Ch double bonds (Ch = S, Se, Te). The formal Bi=Te double bond of the arylbismuthinidene telluride **6BiTe** (bond length 2.7614(4) Å) comprises the heteroatomic combination of the two heaviest main group elements excluding strongly radioactive ones. A bond analysis suggests these formal double bonds are best described as bipolar $^+$Sb–Ch$^-$ and $^+$Bi–Ch$^-$ single bonds (Ch = S, Se, Te).

Author contributions

F. M. synthesized and isolated the compounds **1**, **2**, [**4**]A (A = AlCl$_4$, O$_3$SCF$_3$), **5Pn**, **6PnCh** and performed NMR and UV-vis measurements. A. S. synthesized and performed NMR and UV-vis measurements on **3Pn** and [**4As**][As$_2$OCl$_5$]. J. B. conducted the x-ray diffraction measurements and structure refinement. J. B. and L. D. designed the project. E. H. performed all theoretical computations. Writing of the manuscript was done by F. M., L. D., J. B. and E. H.

Conflicts of interest

There are no conflicts to declare.

Data availability

Figures of NMR spectra as well as crystal and refinement data are given in the supporting information. Crystallographic information files (CIF) have been deposited with the Cambridge Crystallographic Data Centre, nos. 2446710-2446720, 2457652 and 2457653. Additional results from quantum chemical calculations are given in the supporting information. The raw data that support the findings of this study are available from the corresponding authors upon reasonable request.

Acknowledgements

Notes and references

1 L. Dostal, *Coord. Chem. Rev.*, 2017, **353**, 142-158.
2 M. He, C. Hu, R. Wei, X.-F. Wang and L. L. Liu, *Chem. Soc. Rev.*, 2024, **53**, 3896-3951.
3 J. M. Lipshultz, G. Li and A. T. Radesevich, *J. Am. Chem. Soc.*, 2021, **143**, 1699-1721.
4 H. W. Moon and J. Cornella, *ACS Catal.*, 2022, **12**, 1382-1393.
5 Y. Pang, N. Nöthling, M. Leutzsch, L. Kang, E. Bill, M. van Gastel, E. Reijerse, R. Goddard, L. Wagner, D. SantaLucia, S. DeBeer, F. Neese and J. Cornella, *Science*, 2023, **380**, 1043-1048.
6 M. Wu, H. Li, W. Chen, D. Wang, Y. Chen, S. Ye and G. Tan, *Nat. Sci. Rev.*, 2023, **10**.
7 M. Wu, H. Li, W. Chen, D. Wang, Y. He, L. Xu, S. Ye and G. Tan, *Chem*, 2023, **9**, 2573-2584.
8 M. Janssen, T. Frederichs, M. Olaru, E. Lork, E. Hupf and J. Beckmann, *Science*, 2024, **385**, 318-321.
9 D. Wang, W. Chen, H. Chen, Y. Chen, S. Ye and G. Tan, *Nature Chem*, 2025, **17**, 38-43.
10 P. Šimon, F. de Proft, R. Jambor, A. Růžička and L. Dostál, *Angew. Chem. Int. Ed.*, 2010, **49**, 5468-5471.
11 I. Vránová, M. Alonso, R. Lo, R. Sedlák, R. Jambor, A. Růžička, F. de Proft, P. Hobza and L. Dostál, *Chem. Eur. J.*, 2015, **21**, 16917-16928.
12 I. Vránová, M. Alonso, R. Jambor, A. Růžička, M. Erben and L. Dostál, *Chem. Eur. J.*, 2016, **22**, 7376-7380.
13 Y. Pang, M. Leutzsch, N. Nöthling and J. Cornella, *J. Am. Chem. Soc.*, 2020, **142**, 19473-19479.
14 J. Zechovský, E. Kertész, V. Kremláček, M. Hedja, T. Mikysek, M. Erben, A. Růžička, R. Jambor, Z. Benkő and L. Dostál, *Organometallics*, 2022, **41**, 2535-2550.
15 J. Hyvl, W. Y. Yoshida, A. L. Rheingold, R. P. Hughes and M. F. Cain, *Chem. Eur.*, 2016, **22**, 17562-17565.
16 I. Vránová, V. Kremláček, M. Erben, J. Turek, R. Jambor, A. Růžička, M. Alonso and L. Dostál, *Dalton Trans.*, 2017, **46**, 3556-3568.
17 J. Hyvl, W. Y. Yoshida, C. E. Moore, A. L. Rheingold, R. P. Hughes and M. F. Cain, *Polyhedron.*, 2018, **143**, 99-104.
18 V. Kremláček, J. Hyvl, W. Y. Yoshida, A. Růžička, A. L. Rheingold, J. Turek, R. P. Hughes, L. Dostál and M. F. Cain, *Organometallics*, 2018, **37**, 2481-2490.
19 M. T. Nguyen, B. Gabidullin and G. I. Nikonov, *Dalton Trans.*, 2018, **47**, 17011-17019.

20 H. W Moon, F. Wang, K. Bhattacharyya, O. Planas, M. Leutzsch, N. Nöthling, A. A. Auer and J. Cornella, *Angew. Chem. Int. Ed.*, 2023, **62**, 49.

21 I. Vránová, M. Alonso, R. Jambor, A. Růžička, J. Turek and L. Dostál, Chem. Eur. J., 2017, **23**, 2340-2349.

22 M. Kořenkova, V. Kremláček, M. Erben, R. Jirásko, F. de Proft, J. Turek, R. Jambor, A. Růžička, I. Cisařová and L. Dostál, *Dalton Trans.*, 2018, **47**, 14503-14514.

23 J. Zechovský, V. Kremláček, M. Erben, M. Hedja, E. Rychagova, R. Jambor, A. Růžička, S. Ketkov and L. Dostál, *Dalton Trans.*, 2022, **51**, 15933-15945.

24 L. Greb, F. Ebner, Y. Ginzburg and L. M. Sigmund, *Eur. J. Inorg. Chem.*, 2020, **32**, 3030-3047.

25 M. Huang, K. Li, Z. Zhang and J. Zhou, Antimony Redox Catalysis: *J. Amer. Chem. Soc.*, 2024, **146**, 20432-20438.

26 M. Kořenkova, M. Hedja, M. Erben, R. Jirásko, R. Jambor, A. Růžička, E. Rychagova, S. Ketkov and L. Dostál, *Chem. Eur. J.*, 2019, **25**, 12884-12888.

27 M. Hedja, R. Jirásko, A. Růžička, R. Jambor, L. Dostál, *Organometallics*, 2020, **39**, 4320-4328.

28 M. Mato P. C. Bruzzese, F. Takahashi, M. Leutzsch, E. J. Reijerse, A. Schnegg and J. Cornella, *J. Am. Chem. Soc.*, 2023, **145**, 18742-18747.

29 M. Mato, D. Spinnato, M. Leutzsch, H. W. Moon, E. J. Reijerse and J. Cornella, *Nature Chem.*, 2023, **15**, 1138-1145.

30 X. Yang, E. J. Reijerse, K. Bhattacharyya, M. Leutzsch, M. Kochius, N. Nöthing, J. Busch, A. Schnegg, A. A. Auer and J. Cornella, *J. Amer. Chem. Soc.*, 2022, **144**, 16535-16544.

31 X. Yang, E. J. Reijerse, N. Nöthing, D. J. SantaLucia, M. Leutzsch, A. Schnegg and J. Cornella, *J. Amer. Chem. Soc.*, 2023, **145**, 5618-5623.

32 F. Wang, O. Planas and J. Cornella, *J. Amer. Chem. Soc.*, 2019, **141**, 4235-4240.

33 Y. Pang, M. Leutzsch, N. Nöthling, F. Katzenburg and J. Cornella, *J. Am. Chem. Soc.*, 2021, **143**, 12487-12493.

34 V. A. Béland, N. Nöthing, M. Leutzsch and J. Cornella, *J. Am. Chem. Soc.*, 2024, **146**, 25409-25415.

35 T. Tsuruta, D. Spinnato, H. W. Moon, M. Lentzsch and J. Cornella, *J. Am. Chem. Soc.*, 2023, **145**, 25538-25544.

36 S. Ni, D. Spinnato and J. Cornella, *J. Am. Chem. Soc.*, 2024, **146**, 22140-22144.

37 M. Mato, F. Wang and J. Cornella, *Adv. Synth. Catal.*, 2024, **366**, 740-744.

38 M. Olaru, J. F. Kögel, E. Lork, S. Mebs, M. Vogt and J. Beckmann, *Chem. Eur. J.*, 2020, **26**, 275-284.

39 M. Olaru, E. Rychagova, S. Ketkov, Y. Shynkarenko, S. Yakunin, M. V. Kovalenkoc, A. Yablonsiky, B. Andreev, J. Beckmann and M. Vogt, *J. Am. Chem. Soc.*, 2020, **142**, 373-381.

40 F. Meyer, P. Puylaert, D. Duvinage, E. Hupf and J. Beckmann, *Chem. Commun.*, *2024*, **60**, 12912-12915.

41 X. Li, Y. Chen, S. Dong, D. Wang, L. Xu, J. Zhu and G. Tan, *J. Am. Chem. Soc.*, 2025, **147**, 9858–9864.

42 F. Meyer, T. Kuzmera, E. Lork, M. Vogt and J. Beckmann, *Z. Anorg. Allg. Chem.*, 2021, **647**, 1890-1895.

43 I. Vránová, R. Jambor, A. Růžička, R. Jirásko and L. Dostál, *Organometallics*, 2015, **34**, 534-541.

44 I. Vránová, M. Erben, R. Jambor, A. Růžička, R. Jirásko and L. Dostál, *Z. Anorg. Allgem. Chem.*, 2016, **642**, 1212-1217.

45 J. Vrána, R. Jambor, A. Růžička, A. Lyčka, F. De Proft and L. Dostál. *J. Organomet. Chem*. 2013, **723**, 10-14.

46 a) R. Jambor, A. Růžička, A. Lyčka, J. Brus, F. de Proft and L. Dostál, *Organometallics*, 2008, **27**, 6059-6062. b) P. Šimon, R. Jambor, A. Růžička, A. Lyčka, F. De Proft and L. Dostál *Dalton Trans*. 2012, **41**, 5140-5143.

47 S. Heimann, A. Kuczkowski, D. Bläser, C. Wölper, R. Haack, G. Jansen and S. Schulz, *Eur. J. Inorg. Chem.*, 2014, **28**, 4858–4864.

48 P. Šimon, R. Jambor, A. Růžička and L. Dostál, *Organometallics*, 2013, **32**, 239–248.

49 *Complementary Bonding Analysis*; Grabowsky, S., Ed.; de Gruyter: Berlin, 2021.

50 R. W. F. Bader, *Atoms in Molecules. A Quantum Theory*, Cambridge University Press, Oxford U.K., 1991.

51 a) F. Feige, L. A. Malaspina, F. Kleemiss, J. F. Kögel, S. Ketkov, E. Hupf, S. Grabowsky and J. Beckmann, *Dalton Trans.* 2023, **52**, 5918-5925. b) M. Fugel , M. F. Hesse , R. Pal , J. Beckmann , D. Jayatilaka , M. J. Turner , A. Karton , P. Bultinck , G. S. Chandler and S. Grabowsky , *Chem. − Eur. J.*, 2018, **24** , 15275-15286.

52 E. R. Johnson, S. Keinan, P. Mori-Sánchez, J. Contreras-García, A. J. Cohen and W. Yang, *J. Am. Chem. Soc.*, 2010, **132**, 6498-6506.

53 Brent Lindquist-Kleissler, John S. Wenger and Timothy C. Johnstone, *Inorg. Chem.*, 2021, **60**, 1846-1856.

54 a) J. S. Wenger, M. Weng, G. N. George and T. C. Johnstone, *Nat. Chem.*, 2023, **15**, 633−640. b) J. Kuziola, H. W. Moon, M. Leutzsch, N. Nothling, V. A. Beland and J. Cornella, *Angew. Chem. Int. Ed.*, 2024, **64**.

55 Eric D. Glendening, Clark R. Landis and Frank Weinhold, *WIREs Comput. Mol. Sci.*, 2012, **2**, 1–42.

56 M. P. Mitoraj, A. Michalak and T. Ziegler *J. Chem. Theory Comput.*, 2009, **5**, 962-975.

57 a) H. L. Schmider and A. D. Becke *J. Mol. Struct. (THEOCHEM)* 2000, **527**, 51-61; b) V. Tsirelson and A. Stash *Acta Cryst.* 2002, **B58**, 780-785.

Data availability

Figures of NMR spectra as well as crystal and refinement data are given in the supporting information. Crystallographic information files (CIF) have been deposited with the Cambridge Crystallographic Data Centre, nos. 2446710-2446720, 2457652 and 2457653. Additional results from quantum chemical calculations are given in the supporting information. The raw data that support the findings of this study are available from the corresponding authors upon reasonable request.

Chemical Science Accepted Manuscript